06

GaAs/Si buffer structures grown by metal-organic chemical vapor deposition

© S.O. Slipchenko, V.V. Shamakhov, M.I. Kondratov, E.V. Fomin, D.N. Nikolaev, A.V. Myasoedov, N.A. Bert, N.A. Pikhtin

Ioffe Institute, St. Petersburg, Russia
E-mail: serghpl@mail.ioffe.ru

Received November 1, 2025
Revised December 8, 2025
Accepted December 9, 2025

GaAs buffer layers with thicknesses ranging from 1 to 5.3 μm were grown on Si substrates by metalorganic chemical vapor deposition. It is shown that the threading dislocations density decreases to $4 \cdot 10^7$ cm^{-2} with an increase in the GaAs buffer layer thickness up to 5.3 μm. The root mean square surface roughness reaches its minimum value of 2.2 nm at a GaAs buffer layer thickness of 1.6 μm.

Keywords: metal-organic chemical vapor deposition, buffer layers, silicon substrate.

DOI: 10.61011/TPL.2026.04.63200.20553

Si-based photonic integrated circuits (PICs) are being developed rapidly at present, since they offer such advantages as high data transfer rate, low waveguide loss, and low cost [1,2]. However, the indirect-gap structure of silicon makes it somewhat difficult to fabricate efficient and reliable light sources [3]. Light sources based on $A^{III}B^{V}$ compounds—namely, GaAs and InP [4–6]—are well suited for this. At present, the main methods for integrating $A^{III}B^{V}$ materials with silicon are wafer bonding and transfer printing; epitaxial growth of $A^{III}B^{V}$ materials on a Si substrate has also been progressing rapidly [7]. Direct epitaxial growth of $A^{III}B^{V}$ materials has certain advantages over the other two integration methods, since it allows one to produce compact and tightly integrated PICs with high scalability and reduced cost and power consumption [8].

However, direct growth of $A^{III}B^{V}$ compounds (e.g., GaAs and InP) is fraught with a number of difficulties [9]. Among these are a significant mismatch of lattice constants (GaAs — 4.1 %, InP — 8 %) and thermal expansion coefficients (GaAs — $6.6 \cdot 10^{-6}$ K^{-1}, InP — $4.6 \cdot 10^{-6}$ K^{-1}, Si — $2.3 \cdot 10^{-6}$ K^{-1}) between group $A^{III}B^{V}$ materials and Si, which leads to a high density of threading dislocations, the emergence of stacking faults, and the formation of mechanical cracks in the $A^{III}B^{V}$ layer. The lack of an inversion center for $A^{III}B^{V}$ compounds with a zinc blende (sphalerite) structure also leads to the formation of planar crystalline defects of a different type (antiphase boundaries, APBs) during epitaxy on a Si substrate with the (001) orientation. One way to suppress APB formation is to use misoriented substrates [10,11]. Threading dislocations (TDs) are harder to control. A set of measures are implemented for this purpose: multi-stage temperature growth [12,13], thermal cyclic annealing [14,15], and the use of dislocation filters [16–18]. At the same time, the task of growing epitaxial $A^{III}B^{V}$ layers with a low TD density (TDD) on a Si substrate still remains relevant. The optimal design of a buffer in this case is a compromise between the values of TDD and the root mean square roughness (RMSR) of the surface. In addition, the buffer layer should have no macrodefects or cracks.

In the present paper, we report the results of examination of the influence of thickness of a GaAs buffer layer grown on a Si substrate on the TDD and RMSR values. Since both parameters affect the quality of the material and its optical properties, the selection of optimal thickness of the buffer layer based on these two parameters is an important task. The use of the simplest buffer based on GaAs only may be regarded as the most accessible and technologically simple solution. It should also be noted that these studies are the only ones demonstrating the possibility of growth in a metal-organic chemical vapor deposition (MOCVD) setup with a vertical turbodisc reactor.

The MOCVD method was used to form buffer layers. GaAs buffer layers were grown in a vertical turbodisc reactor on Si (001) substrates with a 4° misorientation in the [110] direction. Misoriented Si substrates were chosen as the simplest way to suppress the formation of APBs during the growth of the GaAs buffer layer. Prior to growth, the Si substrate was treated in an aqueous HF solution to remove the natural oxide from its surface. Reagents of group III (trimethylgallium) and group V (arsine) elements were used to grow the GaAs buffer layer. The carrier gas was hydrogen. The growth of GaAs buffer layers was initiated at a reduced temperature (400 °C); in the process of growth, the temperature was then raised to 650 °C, which is optimal for synthesizing GaAs layers with the best structural characteristics. Several samples with different thicknesses of the high-temperature GaAs layer were obtained in the present study: sample No. 1 — 1 μm, sample No. 2 — 1.6 μm, sample No. 3 — 2 μm, and sample No. 4 — 5.3 μm. Their structural characteristics were examined by scanning electron microscopy (SEM), atomic force

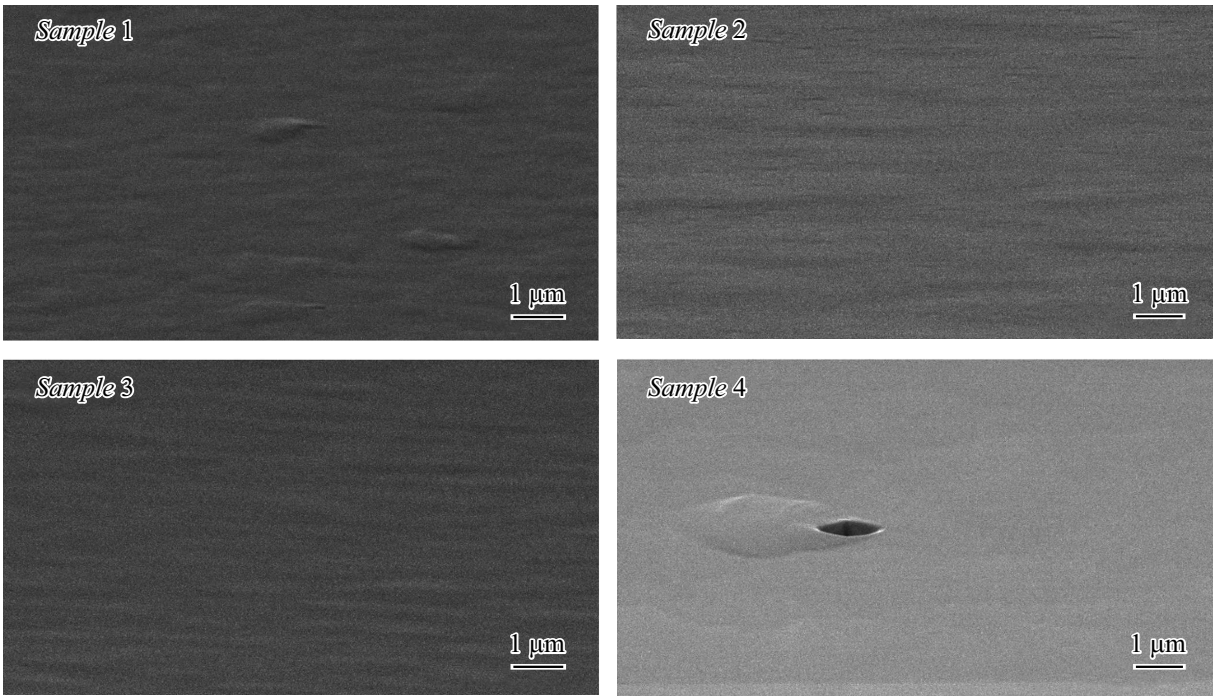

Figure 1. SEM images of the surface of GaAs buffer layers of different thickness: sample No. 1 — 1 μm, sample No. 2 — 1.6 μm, sample No. 3 — 2 μm, and sample No. 4 — 5.3 μm.

microscopy (AFM), and transmission electron microscopy (TEM). The surface morphology was investigated with a JEOL JSM 7001F scanning electron microscope and an NTEGRA (NT-MDT Spectrum Instruments) atomic force microscope in the tapping mode using ETALON HA_FM probes (scanning was performed over a $10 \times 10\,\mu m^2$ area). The TDD was estimated using Philips EM420 and JEM Jeol 2100F transmission electron microscopes at an accelerating voltage of 100 and 200 kV, respectively. Electron-transparent samples were prepared in accordance with the standard procedure that includes cutting, grinding, polishing, and ion sputtering.

Figure 1 shows SEM images of the surfaces of samples obtained under the same magnification. It is evident that all samples have an undulating surface. Qualitative differences in the characteristic surface structure are also noticeable. Sample No. 1, which has the smallest thickness of the GaAs buffer layer, features the most pronounced relief. As the GaAs buffer layer grows thicker, the lateral dimensions of characteristic structural elements forming the surface relief increase. In addition, cracks were detected on the surface of sample No. 4 under lower magnification. These are induced by severe mechanical stresses attributable to a significant difference in thermal expansion coefficient of the Si substrate and the GaAs buffer layer that arise when the structure is cooled from the epitaxy temperature to room temperature. The greater the difference between the growth temperature and room temperature is, the smaller is the critical thickness of the GaAs buffer layer at which cracks start to form. The other samples had no features of this kind.

AFM measurements were performed in order to study the surface morphology of all samples in more detail. Figure 2 shows the AFM images of $10 \times 10\,\mu$m regions of the surface of samples. These images were used to determine the RMSR of the surface, which, along with the TDD, is an important characteristic of the GaAs buffer layer grown on a Si substrate. The measurement results revealed that the RMSR value decreases as the thickness of the GaAs buffer layer increases from 1 to 1.6 μm: sample No. 1 — 4 nm; sample No. 2 — 2.2 nm. However, a further increase in thickness from 1.6 to 5.3 μm is accompanied by an increase in RMSR: sample No. 3 — 2.5 nm; sample No. 4 — 2.9 nm. The root-mean-square error of AFM measurements did not exceed 0.1 nm. In addition, it is fair to assume that dark elongated streaks in the AFM images are TDs. It is evident that the TDD decreases from sample No. 1 to sample No. 4. The TDD values estimated based on the data from Fig. 2 are as follows: sample No. 1 — more than $10^9\,cm^{-2}$, sample No. 2 — $7 \cdot 10^8\,cm^{-2}$, sample No. 3 — $3.1 \cdot 10^7\,cm^{-2}$, and sample No. 4 — $7 \cdot 10^6\,cm^{-2}$.

TEM images of the near-surface section of the GaAs buffer layer prepared in planar geometry were obtained for samples Nos. 3 and 4 (Fig. 3). The TEM method allows for direct measurement of the TDD value in the near-surface region of the buffer layer. In the present study, five images of different regions of the surface were obtained for each sample (in order to suppress the influence of non-uniform distribution of TDs at their low density), and the average TDD was determined based on these images. The TDD varied from $4 \cdot 10^7$ to $1.2 \cdot 10^8\,cm^{-2}$ and from $2.4 \cdot 10^7$ to $7.7 \cdot 10^7\,cm^{-2}$ for samples Nos. 3 and 4, respectively.

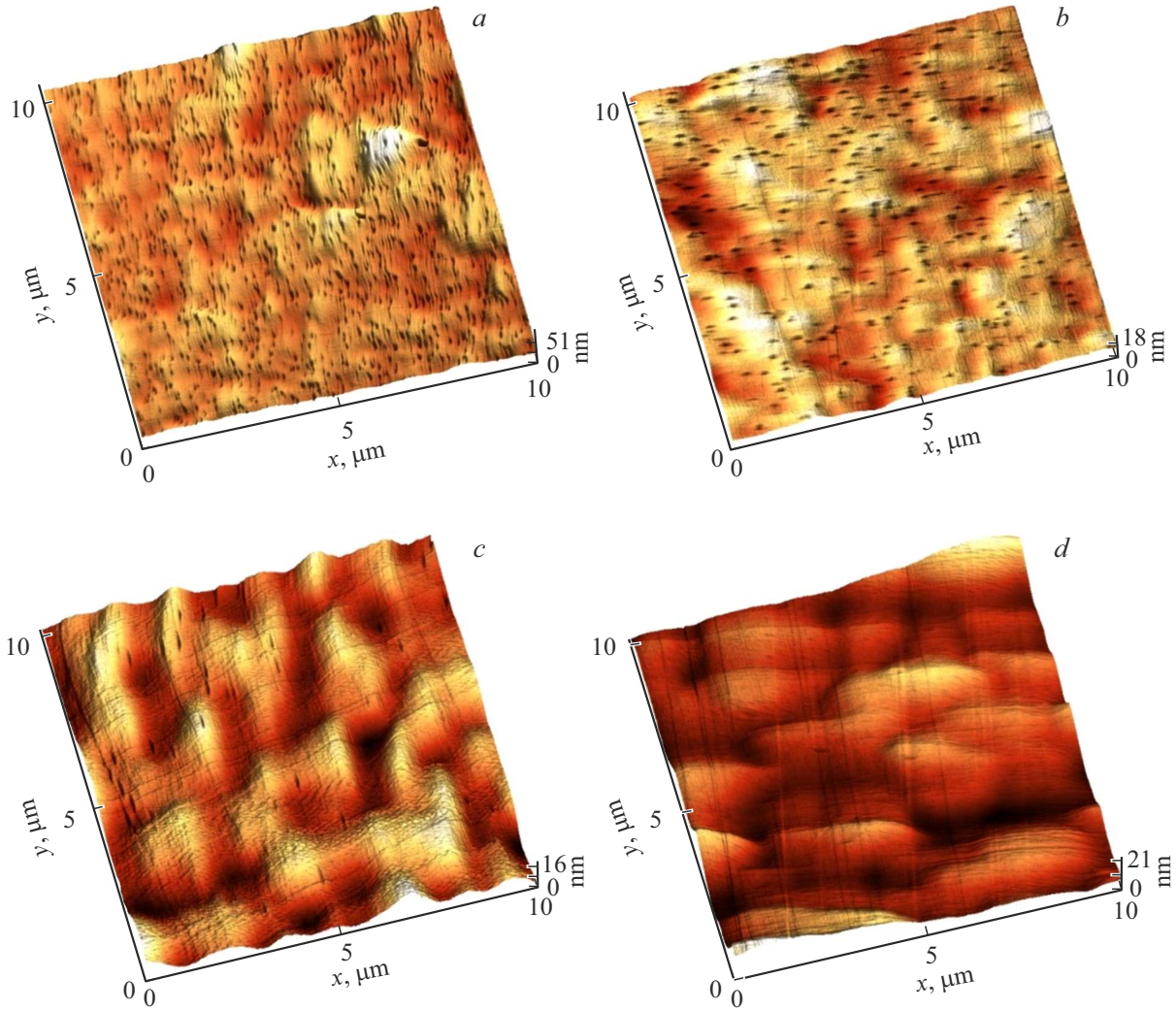

Figure 2. AFM images of the surface of GaAs buffer layers of different thickness: *a* — 1 μm (sample No. 1), *b* — 1.6 μm (sample No. 2), *c* — 2 μm (sample No. 3), and *d* — 5.3 μm (sample No. 4). The scanning area is $10 \times 10\,\mu\text{m}^2$.

The averaged TDD was $7 \cdot 10^7\,\text{cm}^{-2}$ for sample No. 3 and $4 \cdot 10^7\,\text{cm}^{-2}$ for sample No. 4. Comparing the TDD data derived from AFM images to those obtained based on TEM images, one may note that the AFM-based values are lower. This is attributable to the fact that AFM characterizes the epitaxial film surface, while TEM deals with the near-surface region with a thickness up to several hundred nanometers.

One of the mechanisms for reducing TDD is the interaction of TDs with each other. Arrows in the TEM images in Fig. 3 indicate the TD interaction regions in the bulk of the GaAs buffer layer. The interaction of TDs may lead to the formation of mismatch dislocations with a new Burgers vector and reduce the TDD. The light arrow in Fig. 3, *b* points at the region of interaction of two TDs, which resulted in the formation of one mismatch dislocation. A horizontal fragment of the dislocation line is seen in the image. As the TDD decreases with an increase in thickness of the GaAs buffer layer, the degree of interaction between dislocations also decreases.

The obtained results demonstrate that the use of the simplest buffer layer based on GaAs and optimization of its thickness provide an opportunity to reduce the TDD to $4 \cdot 10^7\,\text{cm}^{-2}$. However, the formation of mechanical cracks in a GaAs buffer layer with a thickness of 5.3 μm, which makes it unsuitable for further use, was noted. It was also demonstrated that the RMSR of the GaAs buffer layer surface decreases to 2.2 nm with an increase in thickness to 1.6 μm; as the thickness grows further to 5.3 μm, the RMSR value increases slightly to 2.9 nm.

Based on the obtained results, we chose the GaAs buffer layer with a thickness of 2 μm, which is a compromise in terms of TDD and RMSR values, for further studies. It was also chosen for the fact that a laser structure with quantum wells or quantum dots needs to be grown on the buffer layer, and the total thickness (with the buffer layer included) should ensure that mechanical cracks do not form in the structure. Dislocation filters (DFs) are planned to be used to reduce the TDD in the GaAs buffer layer further. Strained superlattices or sets of bulk strained layers often

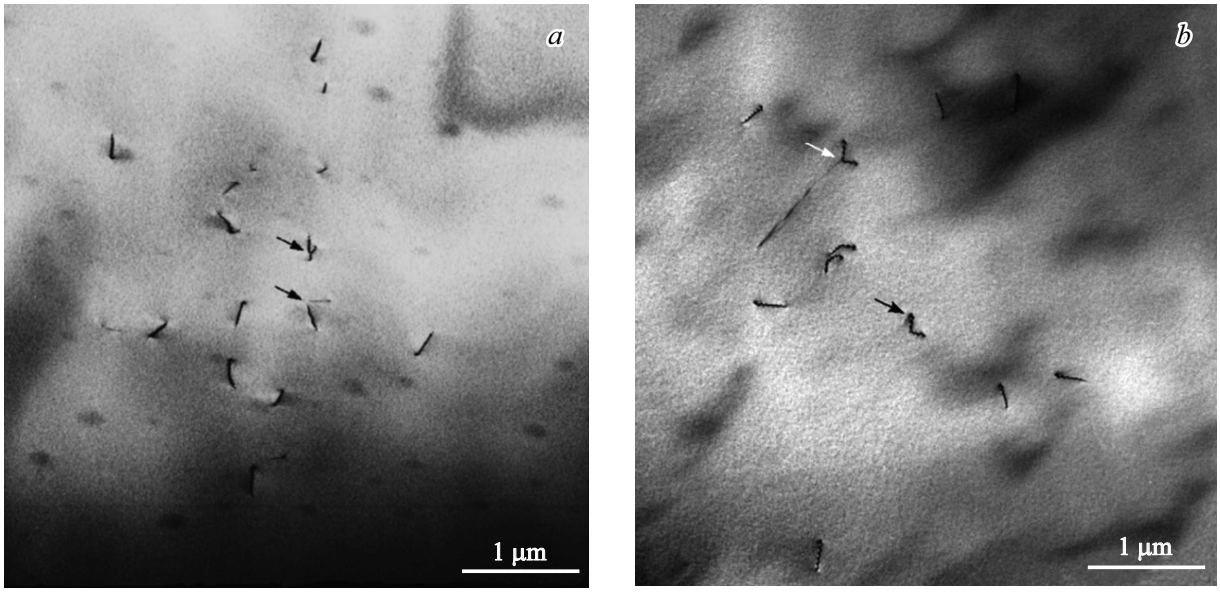

Figure 3. Bright-field TEM images of the section of the GaAs buffer layer in planar geometry obtained near the [001] zone axis. The GaAs buffer layer thickness: *a* — 2 μm (sample No. 3); *b* — 5.3 μm (sample No. 4).

serve as DFs. In most cases, up to four strained superlattices are used. The use of DFs may raise the total thickness of the GaAs buffer layer to 3 μm (depending on the thickness of GaAs separating layers between DFs). The RMSR of such a buffer may increase; according to our estimates, a satisfactory RMSR value in a GaAs buffer layer with a DF is the one that does not exceed 3.5 nm.

Conflict of interest

The authors declare that they have no conflict of interest.

References

[1] J.C. Norman, D. Jung, Y. Wan, J.E. Bowers, APL Photon., **3** (3), 030901 (2018). DOI: 10.1063/1.5021345
[2] J. Yang, M. Tang, S. Chen, H. Liu, Light Sci. Appl., **12** (1), 16 (2023). DOI: 10.1038/s41377-022-01006-0
[3] Y. Han, H. Park, J. Bowers, K.M. Lau, Adv. Opt. Photon., **14** (3), 404 (2022). DOI: 10.1364/AOP.455976
[4] S.O. Slipchenko, D.A. Veselov, V.V. Zolotarev, A.V. Lyutetskii, A.A. Podoskin, Z.N. Sokolova, V.V. Shamakhov, I.S. Shashkin, P.S. Kop'ev, N.A. Pikhtin, Bull. Lebedev Phys. Inst., **50** (4), 494 (2023). DOI: 10.3103/S1068335623160108.
[5] N.A. Volkov, A.Yu. Andreev, I.V. Yarotskaya, Yu.L. Ryaboshtan, V.N. Svetogorov, M.A. Ladugin, A.A. Padalitsa, A.A. Marmalyuk, S.O. Slipchenko, A.V. Lyutetskii, D.A. Veselov, N.A. Pikhtin, Quantum Electron., **51** (2), 133 (2021). DOI: 10.1070/QEL17480.
[6] J.-S. Park, H. Deng, S. Pan, H. Wang, Y. Wang, J. Yuan, X. Zhang, H. Zeng, H. Jia, M. Dang, J. Phys. D, **58** (18), 185101 (2025). DOI: 10.1088/1361-6463/adc275
[7] A.Y. Liu, J. Bowers, IEEE J. Sel. Top. Quantum Electron., **24** (6), 6000412 (2018). DOI: 10.1109/JSTQE.2018.2854542
[8] C. Shang, Y. Wan, J. Selvidge, E. Hughes, R. Herrick, K. Mukherjee, J. Duan, F. Grillot, W.W. Chow, J.E. Bowers, ACS Photon., **8** (9), 2555 (2021). DOI: 10.1021/acsphotonics.1c00707
[9] Y. Du, B. Xu, G. Wang, Y. Miao, B. Li, Z. Kong, Y. Dong, W. Wang, H.H. Radamson, Nanomaterials, **12** (5), 741 (2022). DOI: 10.3390/nano12050741
[10] J. Yang, Z. Liu, P. Jurczak, M. Tang, K. Li, S. Pan, A. Sanchez, R. Beanland, J.-C. Zhang, H. Wang, J. Phys. D, **54** (3), 035103 (2021). DOI: 10.1088/1361-6463/abbb49
[11] J. Yang, P. Jurczak, F. Cui, K. Li, M. Tang, L. Billiald, R. Beanland, A.M. Sanchez, H. Liu, J. Cryst. Growth, **514**, 109 (2019). DOI: 10.1016/j.jcrysgro.2019.02.044
[12] K. Ishida, MRS Online Proc. Library, **91**, 133 (1987). DOI: 10.1557/PROC-91-133
[13] Y. Wang, Q. Wang, Z. Jia, X. Li, C. Deng, X. Ren, S. Cai, Y. Huang, J. Vac. Sci. Technol. B, **31** (5), 051211 (2013). DOI: 10.1116/1.4820914
[14] D. Jung, P.G. Callahan, B. Shin, K. Mukherjee, A.C. Gossard, J.E. Bowers, J. Appl. Phys., **122** (22), 225703 (2017). DOI: 10.1063/1.5001360
[15] C. Shang, J. Selvidge, E. Hughes, J.C. Norman, A.A. Taylor, A.C. Gossard, K. Mukherjee, J.E. Bowers, Phys. Status Solidi A, **218** (3), 2000402 (2020). DOI: 10.1002/pssa.202000402
[16] M. Tang, S. Chen, J. Wu, Q. Jiang, V.G. Dorogan, M. Benamara, Y.I. Mazur, G.J. Salamo, A. Seeds, H. Liu, Opt. Express, **22** (10), 11528 (2014). DOI: 10.1364/OE.22.011528
[17] M. Tang, S. Chen, J. Wu, Q. Jiang, K. Kennedy, P. Jurczak, M.Y. Liao, R. Beanland, A. Seeds, H.Y. Liu, IEEE J. Sel. Top. Quantum Electron., **22** (6), 50 (2016). DOI: 10.1109/JSTQE.2016.2551941
[18] M. Dang, H. Deng, S. Huo, R.R. Juluri, A.M. Sanchez, A.J. Seeds, H. Liu, M. Tang, J. Phys. D, **56** (40), 405108 (2023). DOI: 10.1088/1361-6463/ace36d

Translated by D.Safin